JOURNAL OF GEOPHYSICAL RESEARCH, VOL. 107, NO. A7, 1090, 10.1029/2001JA900169, 2002

On the stability of perpendicular particle drifts in cold magnetoplasmas

A. L. Brinca and F. J. Romeiras
Centro de Física de Plasmas, Instituto Superior Técnico, Lisbon, Portugal

L. Gomberoff
Departamento de Física, Facultad de Ciencias, Universidad de Chile, Santiago, Chile

Received 6 March 2001; revised 31 August 2001; accepted 15 September 2001; published 2 July 2002.

[1] Assessment of the stability of perpendicular particle drifts in cold magnetoplasmas shows that their free energy can stimulate wave activity under various circumstances that include nonoscillatory (aperiodic, purely growing) instabilities and growth with zero-drift thresholds. The theoretical model uses gravity as a means of originating the perpendicular drifts but does not address the stability of the macroscopic plasma-gravity system. It adopts a homogeneous zero-order equatorial-plane configuration with the gravity force perpendicular to the background magnetic field; the wave matrix and dispersion equations are derived for arbitrary directions of propagation and magnetized plasma populations, and the influence of the ignored inhomogeneity of the equilibrium medium on the discussed wave activity is shown to be negligible. Even for atomic hydrogen magnetoplasmas and low frequencies (much smaller than the upper hybrid frequency), instabilities are found for the three principal directions (magnetic field, gravity and drift), with some of them maximizing their growth rates away from these axes. The analysis, to be extended to hot plasmas, incorporates the influence of the background magnetic field on the current-carrying particles, recovers, where appropriate, classical instability results, and can also provide insight to the phenomenology encountered in space environments whose perpendicular currents and particle drifts arise from alternative generating mechanisms. Evaluation of the influence of the neglected inhomogeneity of the zero-order medium indicates that the discussed wave activity persists. *INDEX TERMS:* 2772 Magnetospheric Physics: Plasma waves and instabilities; 7871 Space Plasma Physics: Waves and instabilities; 2752 Magnetospheric Physics: MHD waves and instabilities; *KEYWORDS:* perpendicular drifts, stability, nonoscillatory growth, magnetotail, ring current

1. Introduction

[2] Perpendicular particle drifts and associated currents are a common occurrence in space plasmas. They can usually be found in boundary regions, shocks, and magnetotails, artificially created with the injection of particle beams, and arise from perpendicular forces acting on the particles (of course, particle drifts originated in perpendicular electric fields do not bring about currents). Because they can integrate structures that drastically influence the behavior of the environment (e.g., ring current, geomagnetotail, reconnection, and related phenomenology), the study of their stability has attracted many research efforts whose characteristics are determined by the assumed model for the associated magnetoplasma configuration. The adopted approaches range in complexity from the unmagnetized particle beam model [e.g., *Kintner and Kelley*, 1983], to the thoroughly self-consistent current sheet of Harris [*Harris*, 1962] and its variations [e.g., *Lee and Kan*, 1979]. Needless to say, the increase in the model sophistication tends to impose heavier reliance on numerical solutions and, eventually, contributes to the obfuscation of the underlying physics.

[3] Here we use the gravity force solely as a means of generating the particle drifts: we are not concerned with the configuration stability of a plasma under gravity supported by a magnetic field, as earlier studied by *Kruskal and Schwartzschild* [1954] and others [e.g., *Lehnert*, 1961], or the stability of more complex media such as the magnetospheres of giant planets where the additional consideration of the centrifugal force is mandatory [e.g., *Ferrière et al.*, 1999]. Rather, we look at the free energy source associated with the perpendicular drifts and identify the wave activity that they can feed. As commented upon in the concluding Discussion section, similar configurations have been the subject of stability investigations [e.g., *Mikhailovskii*, 1974] but with different objectives, media structure and therefore distinct results; in particular, cyclotron instability studies in magnetoplasmas with perpendicular currents [e.g., *Lominadze*, 1981] apply to hot plasmas that are not considered in this first stage of the research.

0148-0227/02/2001JA900169

[4] Because we want to start from simple models, and thus benefit from closed form analytical solutions that provide guidance to the behavior of more complex environments, the adopted medium consists of a homogeneous cold magnetoplasma under the influence of a gravity force that is perpendicular to the background magnetic field $\mathbf{B_0}$. The approach thus neglects the magnetic field generated by the zero-order perpendicular currents supported by the particle drifts albeit the effects of the associated, but ignored, inhomogeneity are assessed and shown to be negligible. The assumed geometry occurs in the equatorial planes of planetary magnetospheres although, at this stage, we are not concerned with the modeling of any specific space plasma region. The envisaged next step of the present analysis shall extend the results to the hot magnetoplasma case.

[5] The existence of perpendicular currents in the zero-order state of magnetoplasma implies that the gyrophases of the current carrying particles display some degree of organization. The medium could therefore be characterized as nongyrotropic of the unbalanced type (balanced nongyrotropic distributions, as defined in the next citation and related investigations, yield zero perpendicular currents). The nongyrotropic viewpoint [e.g., *Brinca and Romeiras*, 1998, and references therein] can then be helpful in the stability analysis and was already applied to the study of the Harris current sheet [*Motschmann and Glassmeier*, 1998]. Here we shall not pursue this approach; although we recover general nongyrotropic results (e.g., the implicit unbalanced nongyrotropy brings about coupling among the eigenmodes of gyrotropic parallel propagation [e.g., *Brinca et al.*, 1992]), the assumed cold medium deviates from standard unbalanced nongyrotropy, where the perpendicular current arises from the gyrophase organization of the preexisting perpendicular particle velocities (nonexisting in the cold plasma case), and the nongyrotropic method is not fruitful.

[6] In this work the characterization of the assumed zero-order state, cold magnetoplasma permeated by a perpendicular gravity field, is followed by the derivation of the wave matrix and dispersion equations for arbitrary directions of propagation. With emphasis on the behavior of low (well below the upper hybrid) frequency modes the obtained results are then utilized to study the influence of the magnitude of the perpendicular particle drifts (here introduced by the gravity force) on the complex wave dispersion, starting with the principal directions (background magnetic field, gravity field and drift), proceeding to the principal planes and then looking at other wave vector orientations. In spite of the simplicity of the adopted model, the results show a bewildering variety of instabilities that in some instances are nonoscillatory (also named aperiodic, or purely growing, with zero real frequency and positive growth rate in a nonzero real wave number band) and can start with arbitrarily small drifts; we shall describe in detail the physical mechanism of one of them. Because the adopted approach neglects the zero-order magnetic field generated by the perpendicular currents, we assess the influence of the inherent spatial inhomogeneity and conclude that the encountered wave growths are not suppressed by the medium stratification. The final discussion comments upon the results, mentions potential applications in the realm of space plasmas and outlines the envisaged future research in this problem.

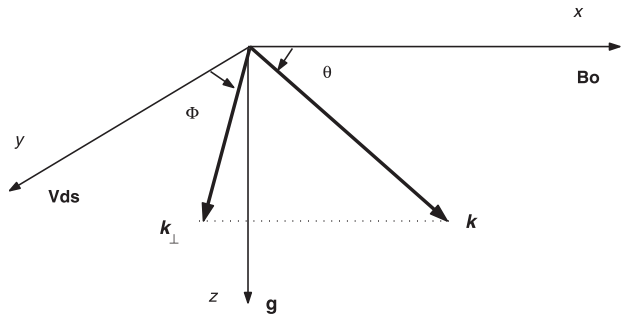

Figure 1. Frame of reference and geometry of the assumed medium.

2. Zero-Order Medium: Wave and Dispersion Equations

[7] The cold magnetoplasma is made up of an arbitrary number of ion species that are neutralized by the electron population; their number densities are denoted by N_s so that in the most commonly investigated case of an H^+ magnetoplasma, $s = e, p$ and $N_e = N_p$. The ambient magnetic field defines the x axis (parallel direction), $\mathbf{B_0} = B_0\ \mathbf{x}$, and the gravity field is aligned with the z axis, $\mathbf{g} = g\ \mathbf{z}$. This configuration, whose geometry is shown in Figure 1, brings about velocity drifts, $\mathbf{V_{ds}} = V_{ds}\ \mathbf{y}$, with (nonrelativistic treatment)

$$V_{ds} = \frac{g}{\Omega_s}, \quad \Omega_s = \frac{q_s B_o}{m_s},$$

where Ω_s represents the (signed angular) cyclotron frequency of species s ($q_e = -e$). The perpendicular current arises from these drifts, with particles of opposite charges moving in opposite directions.

[8] Following, as summarized in Appendix A, a linear perturbation approach in the Maxwell and Lorentz force equations about this zero-order state for first-order quantities varying as $\exp[-i(\omega t - \mathbf{k}\cdot\mathbf{r})]$, with (initial value problem) real wave vector $\mathbf{k}$ (orientation defined by the angles θ and ϕ shown in Figure 1) and $\omega = \omega_r + i\gamma$, yields the wave equation:

$$\left(\frac{k^2c^2}{\omega^2} - 1\right)\mathbf{E} - \frac{c^2}{\omega^2}(\mathbf{k}\cdot\mathbf{E})\mathbf{k} + \frac{\mathbf{J}}{i\omega\varepsilon_0} \equiv \underline{\underline{\mathbf{M}}}\cdot\mathbf{E} = 0,$$

where $\mathbf{E}$ and $\mathbf{J} = \underline{\underline{\sigma}}\cdot\mathbf{E}$ stand for the complex amplitudes of the perturbed electric field and current density, standard notation is used, and the matrix elements M_{ij} are also defined in Appendix A. As usual, the existence of nontrivial wave field solutions implies satisfaction of the dispersion equation

$$D(\omega = \omega_r + i\gamma, \mathbf{k}) \equiv \det\left|\underline{\underline{\mathbf{M}}}\right| = 0,$$

with unstable solutions associating with $\gamma > 0$.

[9] Numerical solutions use $N_e = 15.5$ cm^{-3} and $B_0 = 5$ nT, which could be taken as typical solar wind values at 1 AU, although we reiterate that in this first stage of the investigation, no specific space region is under consideration. Unless stated otherwise, the results relate to a hydrogen plasma where the above parameters imply an Alfvén velocity $v_A = 27.7$ km s^{-1}, electron and proton cyclotron frequencies $|\Omega_e|/2\pi = 140$ Hz and $\Omega_p/2\pi = 76.2$ mHz, a lower hybrid frequency $\omega_{LH} = 42.84\ \Omega_p$, and other characteristic frequencies (upper hybrid, right- and left-hand cutoffs) of the order of the plasma frequency $\omega_{pp} = (e^2 N_p/\varepsilon_0 m_p)^{1/2} = 0.46368 \times 10^6\ \Omega_p$. The dispersion results shall be normalized with respect to Ω_p (real frequencies and growth rates) and Ω_p/v_A (wave numbers), with v_A being used to normalize the (drift) velocities.

3. Reference Medium: Zero Drift

[10] Without particle drifts ($V_{ds} = g = 0$) the model represents a standard cold magnetoplasma whose wave dispersion characteristics are well known and, having no free energy sources or loss mechanisms, yield $\gamma = 0$. This zero-drift state is our reference medium. For parallel propagation ($\theta = 0$), there exist purely electromagnetic modes with right- and left-handed circular polarization, both with two branches. As the wave number increases, the lower-frequency ones start at zero frequency and asymptotically tend to the resonance frequencies $|\Omega_e|$ (right-hand magnetosonic whistler branch) and Ω_p (left-hand Alfvén/ion cyclotron mode). Their high-frequency branches start at the cutoff frequencies (ω_L and ω_R) and asymptotically approach the light dispersion ($\omega_r = kc$). The oscillations at the plasma frequency are not a wave mode. At perpendicular propagation ($\theta = \pi/2$) we find the ordinary mode (starting at the plasma frequency cutoff, ω_p, and tending to the light dispersion) and three branches of the extraordinary mode. The lower-frequency branch starts at zero frequency and asymptotically tends to the lower hybrid resonance ω_{LH}; the intermediate branch starts at the ω_L cutoff and tends to resonance at the upper hybrid frequency, ω_{UH}, and the higher-frequency branch has the same cutoff as the high-frequency right hand parallel mode, ω_R, approaching the light dispersion as the wave number increases.

[11] We shall be concerned with frequencies at least 2 orders of magnitude below the plasma frequency. In this range the low-frequency modes of the reference plasma are the whistler and ion cyclotron modes of parallel propagation, and the lower-frequency extraordinary mode. Figure 2 displays their dispersion in a log-log Brillouin diagram and, for the extraordinary mode, the evolution of the magnitude of the ratio of the longitudinal (parallel to **k**) electrostatic electric field component and the amplitude of the total (electrostatic plus electromagnetic) field, $E_k/E = |\mathbf{E} \cdot \mathbf{k}|/|\mathbf{E}||\mathbf{k}|$. It is clear that the depicted extraordinary mode becomes gradually electrostatic as it approaches resonance; both parallel eigenmodes are purely electromagnetic and thus have $E_k/E = 0$. All the eigenwaves are dispersionless at sufficiently small frequencies (wave numbers), with (phase and group) velocities equal to v_A.

4. Propagation Along the Principal Directions

4.1. Magnetic Field Direction

4.1.1. Magnetized plasma

[12] When the wave vector is aligned with the ambient magnetic field ($\theta = 0$), the matrix $\underline{\underline{M}}$ of the wave equation is denoted by $\underline{\underline{P}}$ and its elements become

$$P_{xx} = -1 + \sum_s \frac{\omega_{ps}^2}{\omega^2}$$

$$P_{xy} = P_{yx} = \sum_s \frac{kV_{ds}}{\omega} \frac{\omega_{ps}^2}{\omega^2}$$

$$P_{xz} = P_{zx} = 0$$

$$P_{yy} = \frac{k^2c^2}{\omega^2} - 1 + \sum_s \left(\frac{\omega_{ps}^2}{\omega^2 - \Omega_s^2} + \frac{k^2 V_{ds}^2 \omega_{ps}^2}{\omega^4} \right)$$

$$P_{yz} = -P_{zy} = i \sum_s \frac{\Omega_s \omega_{ps}^2}{\omega(\omega^2 - \Omega_s^2)}$$

$$P_{zz} = \frac{k^2c^2}{\omega^2} - 1 + \sum_s \frac{\omega_{ps}^2}{\omega^2 - \Omega_s^2},$$

yielding the dispersion equation,

$$P_{xx}P_{yy}P_{zz} - P_{xx}P_{yz}P_{zy} - P_{zz}P_{xy}P_{yx} = 0.$$

Because the electromagnetic eigenmodes of the modified ($V_{ds} \neq 0$) medium for parallel propagation are no longer the left- and right-hand circularly polarized modes, no simplification arises in the elements of the matrix of the wave equation with the introduction of "gyrating coordinates" of the symbolic form $(\ )_\pm = [(\ )_y \pm i(\ )_z]/2$ [e.g., *Brinca et al.*, 1993]; the dispersion equation, of course, is independent of the choice of coordinates.

[13] For a hydrogen plasma ($s = e$ and p) the two parallel low-frequency eigenmodes of the zero-drift magnetoplasma, right- and left-hand circularly polarized, are mildly affected by the introduction of the gravity field and associated velocity drifts. As shown in Figure 3, solution of the dispersion equation for proton drift velocities (normalized with respect to v_A) of 1 and 43, the whistler and ion cyclotron branches remain stable, but their real frequencies are moderately modified.

[14] A more interesting effect of the gravity-originated drifts at parallel propagation is shown in Figure 4. As soon as the drift starts for arbitrarily small g, beginning with zero growth at the origin, we find nonoscillatory instabilities (that is, positive growth rates and zero real frequencies in a nonzero wave number band) in the whole wave number domain; the growth rates saturate as k increases at values that scale with the drift speeds. More precisely, the evolution of the growth rates for different drift regimes shows that $\gamma/\Omega_p \rightarrow V_{dp}/v_A$ as $k \rightarrow \infty$.

[15] This asymptotic behavior can be easily confirmed analytically. Noticing that (1) the frequency remains finite

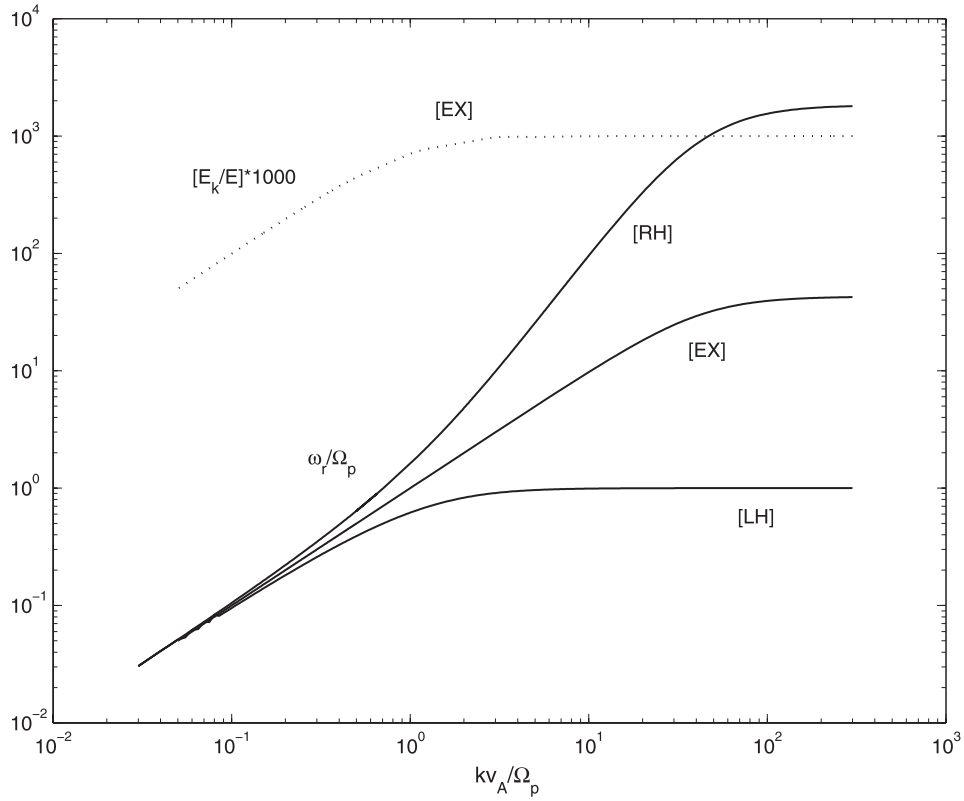

Figure 2. Dispersion of the lowest-frequency eigenmodes in the cold hydrogen magnetoplasma without gravity: right-hand parallel propagating whistler mode [RH], left-hand parallel propagating ion cyclotron mode [LH], and perpendicular propagating extraordinary mode [EX]. Also shown for the [EX] mode, the ratio E_k/E of the electrostatic component of the wave electric field and the magnitude of the total wave electric field.

as the wave number increases, (2) the magnitude of the electron drift speed is 3 orders of magnitude smaller than that of the proton population, and (3) we are looking at the $k \to \infty$ regime, the dispersion equation in this limit becomes

$$P_{xx}P_{yy}P_{zz} - P_{zz}P_{xy}P_{yx} \approx 0,$$

where

$$P_{xx}P_{yy}P_{zz} \approx \frac{k^4c^4\omega_{pe}^2}{\omega^6}\left(1 + \frac{\omega_{pp}^2 V_{dp}^2}{\omega^2 c^2}\right),$$

$$P_{zz}P_{xy}P_{yx} \approx \frac{\omega_{pp}^4 k^4 c^2 V_{dp}^2}{\omega^8}.$$

Recalling that $\omega_{pp}^2/c^2 \approx \Omega_p^2/v_A^2$, we obtain

$$\frac{\omega^2}{\omega_{pp}^2} \approx -\left(\frac{\Omega_p V_{dp}}{\omega_{pp} v_A}\right)^2,$$

or, in agreement with the behavior displayed in Figure 4,

$$\frac{\gamma}{\Omega_p} \approx \frac{V_{dp}}{v_A}.$$

The physical mechanism of this instability whose nonzero perturbed fields for large k can be described by

$$E_y \sim E_{y0}\cos kx\, e^{\gamma t}, \quad B_z \sim \frac{kE_{y0}}{\gamma}\sin kx\, e^{\gamma t},$$

is directly derivable from a few basic equations. (For simplicity, we shall consider an atomic hydrogen plasma.)

1. Let us assume a perturbation along x of the electron and proton densities that preserves charge neutrality ($\rho = \rho_e + \rho_p = 0$, $n_e = n_p$) of the form

$$n_s \sim \cos kx (s = e, p),$$

and follow the ensuing chain of events.

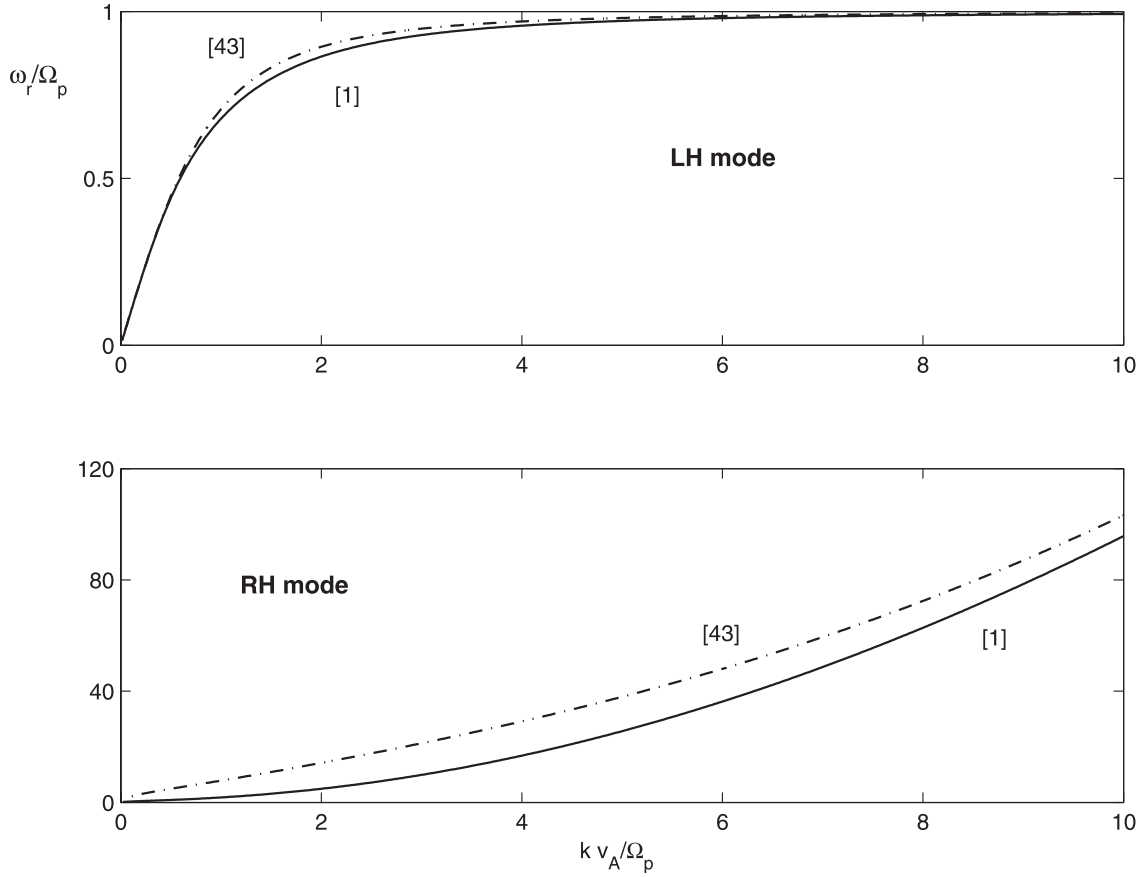

Figure 3. Comparison of the real dispersions of the parallel propagating (top) LH and (bottom) RH modes for normalized proton drift velocities of $V_{dp}/v_A = 1$ and 43.

2. The expression for the perturbed current density, $\mathbf{J}_s = q_s N_s \mathbf{v}_s + q_s n_s V_{ds}\mathbf{y}$, shows that the assumed density perturbation generates

$$J_y = J_{ey} + J_{py} \approx J_{py} \sim \cos kx.$$

(Notice that $J_{sy} = q_s N_s v_{sy} + q_s n_s V_{ds}$ is made up of two terms; the first time we go through this feedback loop, because we prepared the initial system with perturbations only in the densities, and hence $v_{sy} = 0$, the first term is zero. Following times, with wave fields already stimulated, the perturbed velocity is no longer zero; however, the force and continuity equations together with Faraday's law allow us to estimate $|(n_s V_{ds})/(N_s v_{sy})| \approx (kV_{ds}/\gamma)^2 \ [1 + (\Omega_s/\gamma)^2]$ so that, as used above, the second term of J_{sy} is always dominant in the range under investigation. Note, also, that with the adopted conventions we always have $q_s V_{ds} > 0$.)

3. From the generalized Ampère's law this current density perturbation brings about a perturbed electric field,

$$E_y \sim -\cos kx.$$

4. This "wave" electric field, from Faraday's law, induces a wave magnetic field,

$$B_z \sim -\sin kx,$$

and, from the x component of the force equation, $\dot{v}_{sx} = (q_s/m_s)V_{ds}B_z$, creates spatial variations in the perturbed parallel accelerations and velocities of the form,

$$\dot{v}_{sx}, v_{sx} \sim -\sin kx.$$

5. This perturbed parallel velocity feeds a perturbed parallel current density $J_{sx} \sim -\sin kx$, whose spatial inhomogeneity satisfies,

$$\frac{\partial J_{sx}}{\partial x} \sim -\cos kx.$$

6. The continuity equation, $\partial J_{sx}/\partial x + \gamma n_s q_s = 0$, shows that the above current density divergence associates with density perturbations varying as $n_s \sim \cos kx$.

[16] We are thus back at the starting point, having closed a loop with positive feedback that results in the enhancement of the original perturbation and therefore in instability.

[17] In a nutshell, revisiting the growth mechanism and retaining the main contributions, we realize that this instability arises from the ion drift. This flow generates a current density perturbation $J_y \sim n_p V_{dp}$ whose ion density perturbation n_p, being driven by the wave Lorentz force $\sim V_{dp}B_z$, has spatial variations in antiphase with those of the wave electric field ($n_p \sim -\partial J_{px}/\partial x \sim -\partial v_{px}/\partial x \sim -V_{dp}\partial B_z/\partial x \sim V_{dp}\partial^2 E_y/\partial x^2 \sim -V_{dp}E_y$). Thus the

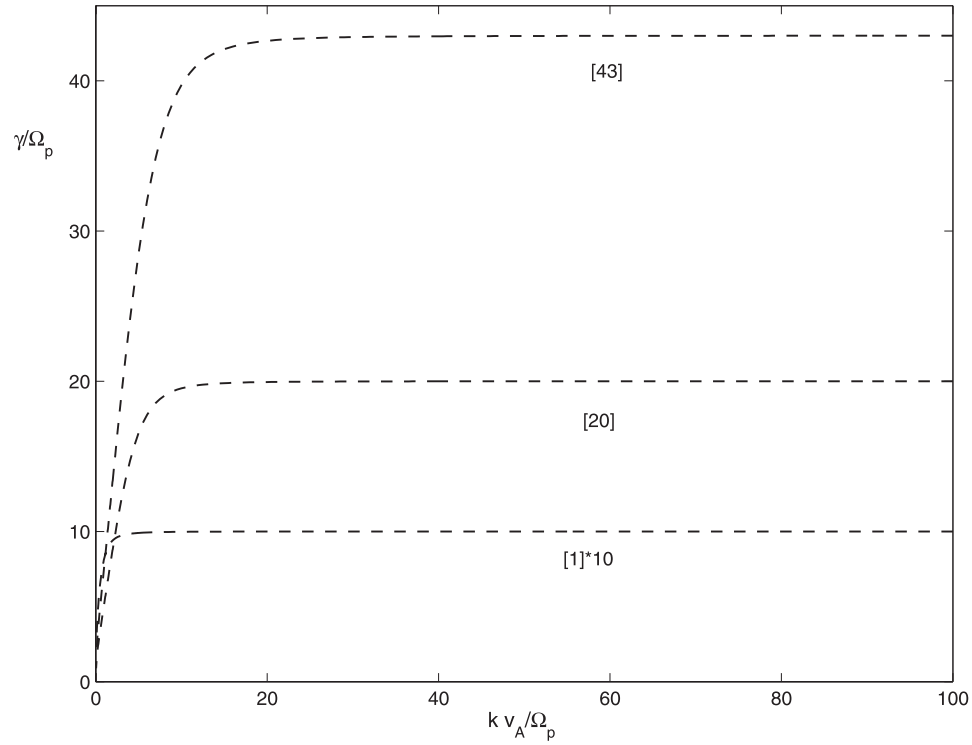

Figure 4. Growth rates of the parallel propagating purely growing mode for normalized proton drift velocities of V_{dp}/v_A = 1, 20, and 43.

free energy in the ion drift can feed the wave growth via this negative power "dissipation" in the medium:

$$\mathbf{J}.\mathbf{E} = J_y E_y \sim -\cos^2 kx < 0\,.$$

4.1.2. Unmagnetized plasma

[18] Because, as shown in the sequel (Figure 12, in particular, and related discussion), this instability is also associated with wave growth encountered for arbitrary directions of propagation contained in the *yz* plane, we further dwell on its phenomenology and demonstrate that the same basic growth mechanism takes place in isotropic ($B_0 = 0$) zero-gravity plasmas with arbitrary collinear particle streams regardless of the (in)existence of a finite zero-order current (and therefore concurrent zero-order magnetic field). The unavoidable inference in the present context is that this parallel nonoscillatory instability is solely due to the free energy in the perpendicular drifts, having nothing to do with the (in)existence of gravity, and the neglect of the zero-order magnetic field generated by the particle drifts. (The possibility that the discarded spatial variations of the zero-order medium could quench this instability is eliminated by the analysis provided in section 6.)

[19] We thus analyze now the stability of cold isotropic plasmas, without a gravity field but supporting collinear streaming populations, with respect to wave propagation perpendicular to the stream direction. Although these streams might sustain a finite zero-order current, we neglect the associated zero-order magnetic field, meaning that the linear study is only exact when the assumed particle drifts bring about a total zero current. We shall find that regardless of the (in)existence of a finite zero-order current, the medium, for the envisaged propagation, is always purely growing unstable through a physical mechanism that coincides with the one described above for the nonoscillatory instability depicted in Figure 4. The finding demonstrates that this aperiodic instability is independent of the neglected magnetic field (originated by the finite zero-order perpendicular current); its occurrence relies solely on the existence of particle (perpendicular, in the main body of the paper) drifts, without regard for the mechanism that generates them.

[20] We assume an isotropic homogeneous cold plasma made up of three populations that are allowed to drift along a common direction taken as the *y* axis: electrons (*e*), protons (*p*), and single ionized ions (*i*), $N_e = N_p + N_i$. The approach is directly applicable to more general conditions but, for simplicity, only the positive-charge species are allowed to drift, originating a zero-order current density $\mathbf{J_0} = e(N_p V_{dp} + N_i V_{di})\,\mathbf{y}$. We shall demonstrate for $\mathbf{k} = k\mathbf{x}$, both when $\mathbf{J_0} = 0$ (exact analysis) and $\mathbf{J_0} \neq 0$ (approximate analysis, as in the remaining body of the paper), that the aperiodic instability under study always takes place.

[21] The space-time dependence of the plane wave perturbations is taken as exp $[-i(\omega t - kx)]$. The continuity and force equations, $kJ_{sx} = \omega q_s n_s$ and $-i\omega m_s \mathbf{v} = q_s\mathbf{E} + q_s(kV_{ds}/\omega)E_y\mathbf{x}$, lead to the current densities,

$$\begin{aligned}\mathrm{J}_s &= q_s N_s \mathbf{v}_s + q_s N_s \frac{kV_{ds}}{\omega} v_{sx} y \\ &= i\varepsilon_0 \frac{\omega_{ps}^2}{\omega}\mathbf{E} + i\epsilon_0 \frac{\omega_{ps}^2}{\omega}\frac{kV_{ds}}{\omega}E_y\mathbf{x} \\ &+ i\varepsilon_0 \frac{\omega_{ps}^2}{\omega}\frac{kV_{ds}}{\omega}\left(E_x + \frac{kV_{ds}}{\omega}E_y\right)\mathbf{y}\end{aligned}$$

that determine the total perturbed current density

$$\begin{aligned}\mathbf{J} &= \mathbf{J}_e + \mathbf{J}_p + \mathbf{J}_i \\ &= i\varepsilon_0 \frac{\omega_p^2}{\omega}\mathbf{E} + i\frac{\varepsilon_0 k}{\omega^2}\left(\omega_{pp}^2 V_{dp} + \omega_{pi}^2 V_{di}\right)\left(E_y\mathbf{x} + E_x\mathbf{y}\right) \\ &\quad + i\frac{\varepsilon_0 k^2}{\omega^3}\left(\omega_{pp}^2 V_{dp}^2 + \omega_{pi}^2 V_{di}^2\right)E_y\mathbf{y}.\end{aligned}$$

Substitution of this total current density into the wave equation,

$$\mathbf{E} - \frac{k^2c^2}{\omega^2}\left(\mathbf{E} - E_x\mathbf{x}\right) = \frac{1}{i\omega\varepsilon_0}\mathbf{J},$$

yields the wave matrix equation. As usual, the dispersion equation (DR) is obtained by imposing that the determinant of the square matrix that multiplies the electric field column matrix be equal to zero.

[22] In the case under analysis we obtain two eigenmodes.

[23] The first one has the electric field linearly polarized along the z axis and satisfies the well-known (''ordinary'' mode) DR,

$$\frac{k^2c^2}{\omega^2} = 1 - \frac{\omega_p^2}{\omega^2}, \quad \omega_p^2 = \omega_{pe}^2 + \omega_{pp}^2 + \omega_{pi}^2.$$

The new hybrid (both electrostatic and electromagnetic components) mode has finite E_x and E_y, and satisfies the DR,

$$\left(1 - \frac{\omega_p^2}{\omega^2}\right)\left[1 - \frac{k^2c^2}{\omega^2} - \frac{\omega_p^2}{\omega^2} - \frac{k^2}{\omega^4}\left(\omega_{pp}^2 V_{dp}^2 + \omega_{pi}^2 V_{di}^2\right)\right] - \frac{k^2}{\omega^6}\left(\omega_{pp}^2 V_{dp} + \omega_{pi}^2 V_{di}\right)^2 = 0.$$

Looking at the dispersion for large k (recall the characteristics of the mode depicted in Figure 4) and recognizing that

$$c^2 \gg V_{dp}^2, V_{di}^2, \quad \omega_{pe}^2 \gg \omega_{pp}^2, \omega_{pi}^2$$

leads to the (purely growing unstable) root

$$-\omega^2 = \gamma^2 \approx \frac{1}{c^2}\left(\omega_{pp}^2 V_{dp}^2 + \omega_{pi}^2 V_{di}^2\right).$$

The growth rate depends on parameters associated with the drifting populations. It is clear that we could have adopted, for example, $i = p$, $N_p = N_i = N_e/2$, $V_{di} = -V_{dp}$, $\mathbf{J_0} = 0$, and obtain the same instability within a completely self-consistent and exact linear analysis (no zero-order current, no zero-order neglected magnetic field).

[24] However, in this case, since $\omega_{pp}^2 V_{dp} + \omega_{pi}^2 V_{di} = 0$, the E_x and E_y components decouple, so that the unstable mode (associated with E_y) is purely ''electromagnetic'' and E_x can only be different from zero when (uninteresting electrostatic cold plasma oscillations) $\omega^2 = \omega_p^2$. Notice that this is the situation that naturally occurs in the magnetoplasma permeated by gravity (take an atomic hydrogen plasma) because the particle drifts satisfy $\omega_{pp}^2 V_{dp} + \omega_{pe}^2 V_{de} = 0$, decoupling also E_x and E_y.

[25] Hence, recalling the above described physical mechanism, noting that the growth rate estimate neglected the electron drift velocity, and using the magnetoplasma relation $v_A \approx (\Omega_p/\omega_{pp})c$, we conclude that the instabilities discussed in the isotropic plasma and in the context of Figure 4 are identical. They have nothing to do, though, with the classical electrostatic streaming (two-stream included) instabilities where the wave vector is aligned with the drifts.

4.2. Drift Direction

[26] The wave vector is now aligned with the y axis ($\theta = \pi/2$, $\phi = 0$). Denoting by $\underline{\underline{\mathbf{D}}}$ the corresponding matrix of the wave equation, we find that its elements become

$$D_{xx} = \frac{k^2c^2}{\omega^2} - 1 + \sum_s \frac{\omega_{ps}^2}{\omega^2}$$

$$D_{xy} = D_{yx} = D_{xz} = D_{zx} = 0$$

$$D_{yy} = -1 + \sum_s \frac{\omega_{ps}^2}{\omega_s^2 - \Omega_s^2}$$

$$D_{yz} = -D_{zy} = i\sum_s \frac{\Omega_s\omega_{ps}^2}{\omega\left(\omega_s^2 - \Omega_s^2\right)}$$

$$D_{zz} = \frac{k^2c^2}{\omega^2} - 1 + \sum_s \frac{\omega_{ps}^2}{\omega^2}\frac{\omega_s^2}{\omega_s^2 - \Omega_s^2}$$

with $\omega_s = \omega - kV_{ds}$.

[27] The (high frequency) ordinary mode, linearly polarized with electric field along the ambient magnetic field, is not affected by the introduction of gravity drifts and maintains its dispersion, $D_{xx} = 0$. The extraordinary mode, in general with electrostatic and electromagnetic electric field components along the y axis and the z axis, respectively, is influenced by the drifts. The ensuing discussion is based on the (low frequency) solutions of the dispersion equation $D_{yy}D_{zz} - D_{yz}D_{zy} = 0$ and revisits manifestations of phenomenology associated with beam-plasma interactions modified by the (perpendicular) orientation of the ''beam'' with respect to the ambient magnetic field [e.g., *Wu et al.*, 1983].

[28] Looking at the real dispersion of the zero-drift extraordinary mode shown in Figure 2 and the dominant (electrostatic) orientation of its wave electric field (along the ion drift direction), we can anticipate that a particle beam ''injected'' along $\mathbf{y}$ with velocity V_{db} might strongly interact with the original extraordinary mode in a region where this beam velocity matches the wave phase velocity, $\omega_r/k \approx V_{db}$: the ensuing wave-particle resonance might then bring about wave growth.

[29] One simple way of introducing this interaction within the adopted model is to consider a dilute population of ions (preferably heavy ions, in order to reduce the concurrent drift speeds of the main electron and proton populations). For example, ions with a drifting velocity of the order of $v_A/2$ would approximately match the extraordinary mode phase velocity around $kv_A/\Omega_p \approx 80$ (see Figure 2). If the resonant particles were O^+ ions, these conditions would imply a moderate proton drift of $V_{dp}/v_A = 0.03125$ (= 0.5/16) and

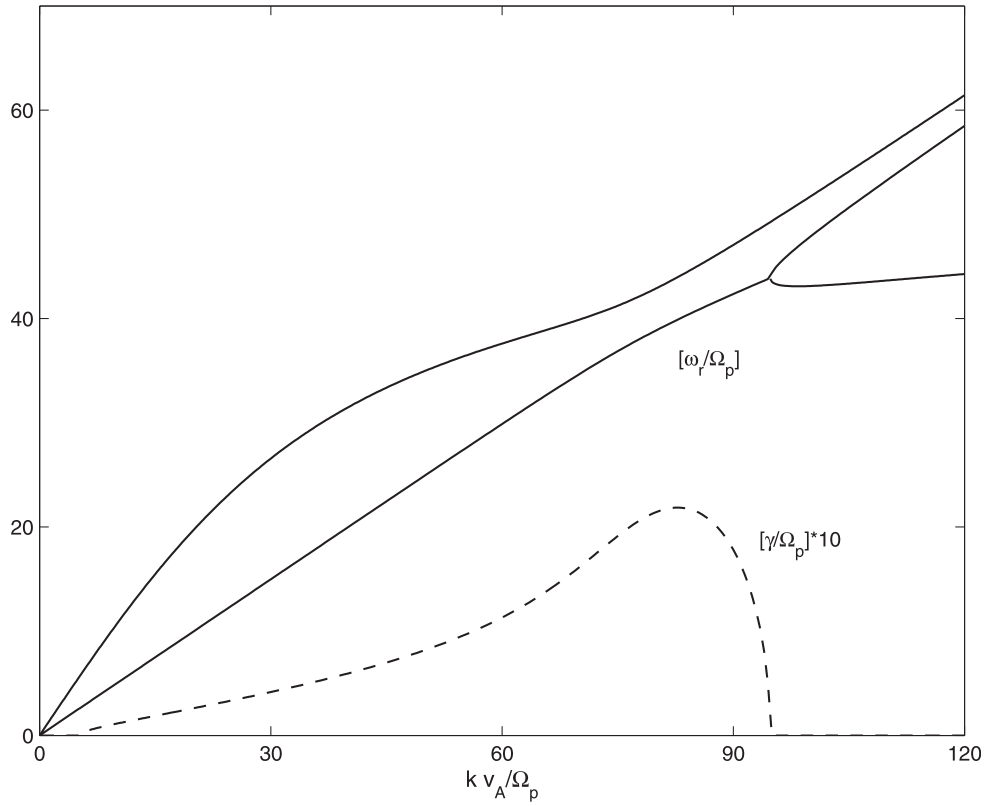

Figure 5. Low-frequency complex dispersion originated in the introduction of an O^+ population (N_{O+} = 0.01 N_e and $V_{dO+} = 0.5v_A$) in the magnetoplasma permeated by a gravity field. The depicted instability along the drift direction arises from the interaction between the oxygen ions and the modified, low-frequency, extraordinary mode.

a negligible electron drift. Figure 5 depicts the consequences of introducing in the magnetoplasma a dilute oxygen population with $N_{O\ +}$ = 0.01 N_e (overall neutrality is maintained through a corresponding reduction in the proton number density). As expected, these heavy resonant ions do interact with the modified extraordinary mode and destabilize the medium, with maximum growth rate occurring around $kv_A/\Omega_p \approx 80$.

[30] In the realm of cold plasmas (that are unable to support Bernstein waves), this situation is similar to the problem studied by *Kintner and Kelley* [1983] of injection of a Xe^+ ion beam in the *F* region of the ionosphere; they assumed that the injected ions were unmagnetized, meaning that the approach can only describe phenomenology with time scales much shorter than the ion cyclotron period. Here, with the limitation of the cold plasma model that we plan to forsake in the next stage of the investigation, the validity of the analysis is not affected by these timescales because all particle populations are magnetized.

[31] Returning to the pure hydrogen magnetoplasma permeated by a gravity field and keeping the wave vector aligned with the drift direction, we now assess the effects of the magnitude of the drift velocities on the wave stability. The configuration resembles a two-stream system or, in the adopted frame of reference (differing little from the electron drift frame), a "beam-plasma" system. The results shown in Figure 6 for proton drift speeds of V_{dp}/v_A = 1, 20, 40, and 43 confirm this perspective: the real dispersion is beam-like, the instability onset takes place for wave number values that decrease with the increase of the drift velocity (for the lowest considered normalized proton drift velocity, 1, the critical normalized wave number is 1834.6, whereas the normalized proton drift velocity of 43 originates wave growth that starts at zero wave number), and the growing modes, as shown in the evolution of the electrostatic component of the wave electric field, become electrostatic as the wave number increases. This behavior, however, is not asymptotic: as the real frequency increases with *k*, it eventually attains values in the domain of other characteristic magnetoplasma frequencies (ω_L, ω_p, ω_{UH}, ω_R), the beam-like dispersion is lost and the instability is quenched.

4.3. Gravity Field Direction

[32] We take the wave vector aligned with the *z* axis ($\theta = \pi/2$, $\phi = \pi/2$) and denote the corresponding matrix of the wave equation by $\underline{\underline{\mathbf{G}}}$. Its elements become

$$G_{xx} = \frac{k^2c^2}{\omega^2} - 1 + \sum_s \frac{\omega_{ps}^2}{\omega^2}$$

$$G_{xy} = G_{yx} = G_{xz} = G_{zx} = 0$$

$$G_{yy} = \frac{k^2c^2}{\omega^2} - 1 + \sum_s \frac{\omega_{ps}^2}{\omega^2 - \Omega_s^2}\left(1 + \frac{k^2V_{ds}^2}{\omega^2}\right)$$

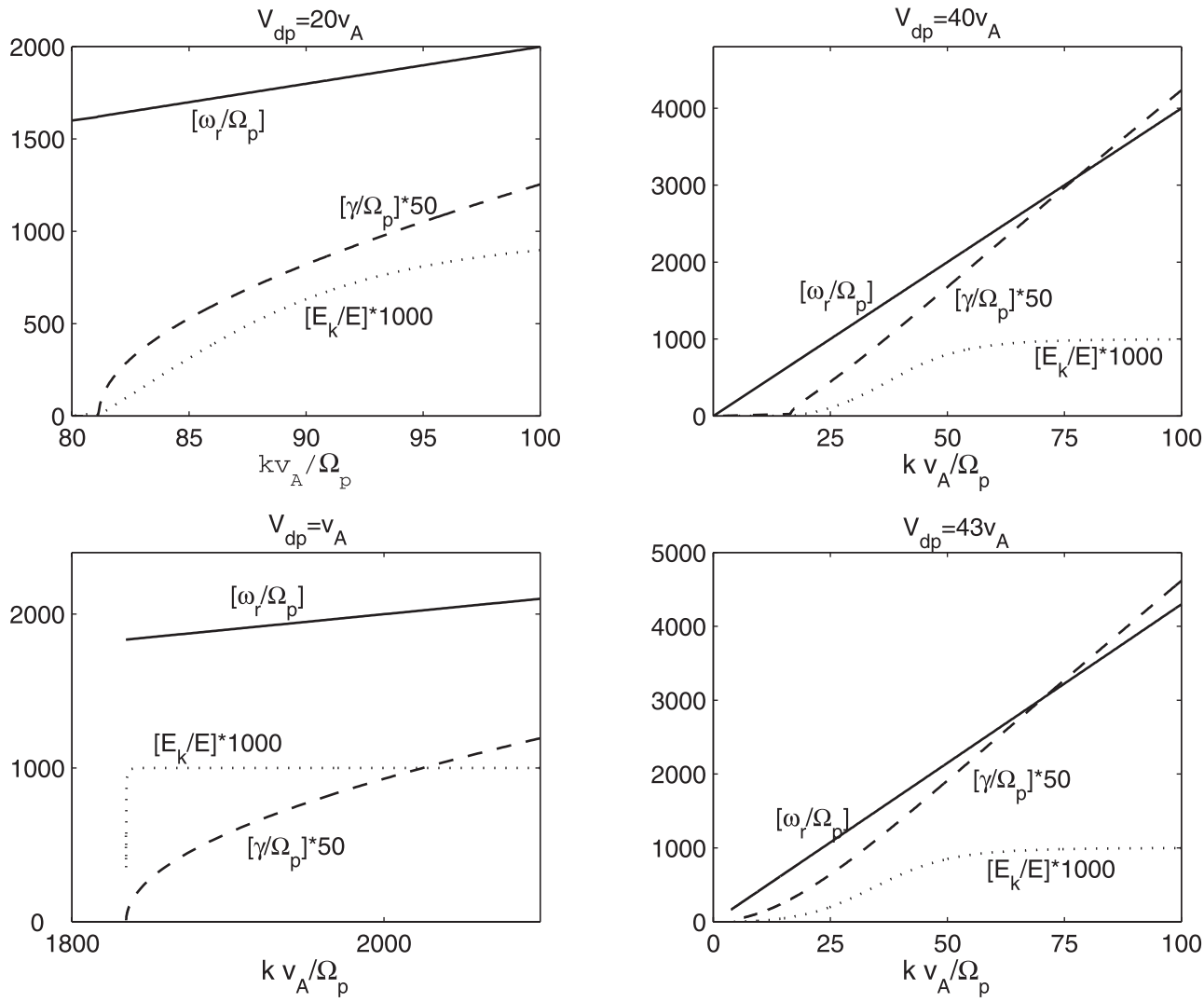

Figure 6. Complex dispersion for propagation along the drift direction at different drift velocities. As the wave number increases, the unstable mode intensifies its electrostatic component. Clockwise starting at the bottom left panel, V_{dp}/v_A = 1, 20, 40, and 43.

$$G_{yz} = \sum_s \frac{\omega_{ps}^2}{\omega^2 - \Omega_s^2}\left(\frac{kV_{ds} + i\Omega_s}{\omega}\right)$$

$$G_{zy} = \sum_s \frac{\omega_{ps}^2}{\omega^2 - \Omega_s^2}\left(\frac{kV_{ds} - i\Omega_s}{\omega}\right)$$

$$G_{zz} = -1 + \sum_s \frac{\omega_{ps}^2}{\omega^2 - \Omega_s^2}$$

The ordinary mode electric field (parallel to the ambient magnetic field) is again perpendicular to the drift direction and thus is not affected by the introduction of the gravity field; its well-known dispersion equation, $G_{xx} = 0$, is not modified. In contrast, the dispersion equation of the modified extraordinary mode, $G_{yy}G_{zz} - G_{yz}G_{zy} = 0$, is strongly influenced by the magnitude of the drift.

[33] Figure 7 depicts the evolution of the low-frequency branch of the extraordinary mode as the proton drift velocity goes from $V_{dp} = v_A$ to $V_{dp} = 43v_A$. As the magnitude of the drift increases, the real frequency curve $\omega_r(k)$ approaches the k axis (the resonance frequencies decrease); at a certain threshold value for the drift (near $V_{dp}/v_A \approx 42.8$), the frequency is zero, with further increases of the drift velocities bringing about a nonoscillatory instability with zero real frequency and positive growth rate in the whole wave number domain. This behavior can be justified analytically and the critical drift values defined.

[34] Bearing in mind the consequences of having $m_p \gg m_e$ and that the frequency remains finite as $k \to \infty$, we find for the asymptotic regime

$$G_{yy}G_{zz} \approx \left(\frac{k^2c^2}{\omega^2} + \frac{k^2V_{dp}^2}{\omega^2}A_p\right)(A_e + A_p - 1)$$

$$G_{yz}G_{zy} \approx A_p^2\frac{k^2V_{dp}^2}{\omega^2}$$

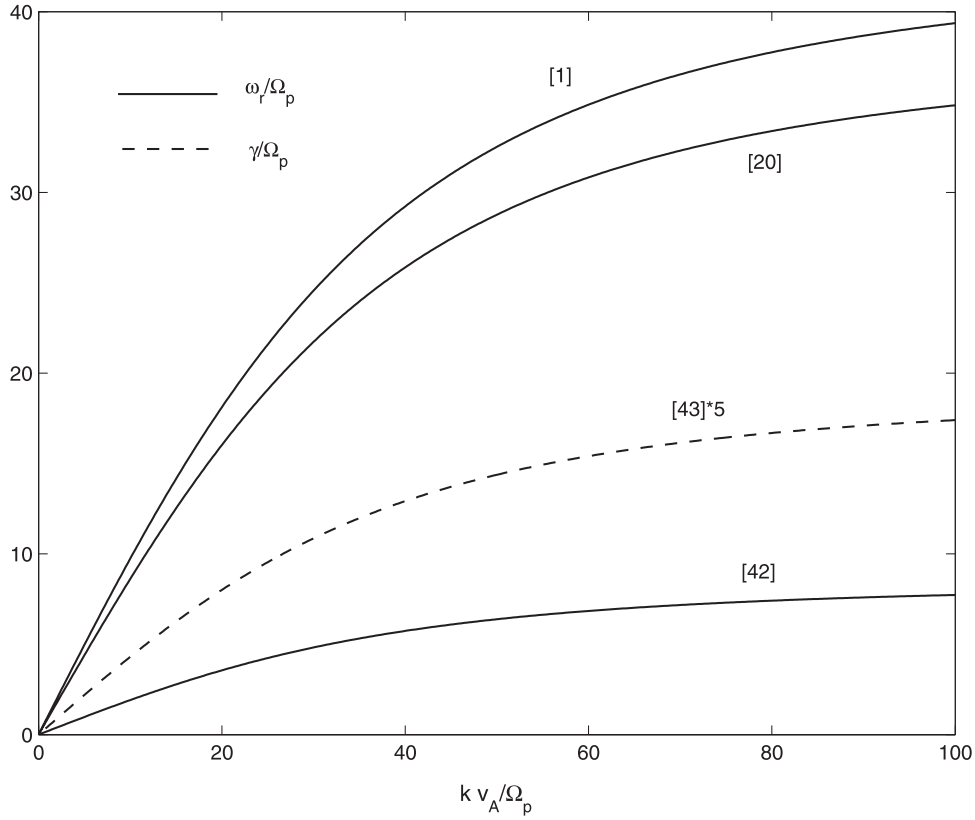

Figure 7. Dispersion for propagation along the gravity force at different drift velocities, $V_{dp}/v_A = 1$, 20, 42, and 43. Above the drift threshold $V_{dp}/v_A \approx (m_p/m_e)^{1/2}$, there occurs the onset of a purely growing mode.

with

$$A_e = \frac{\omega_{pe}^2}{\omega^2 - \Omega_e^2} \approx -\frac{\omega_{pe}^2}{\Omega_e^2}, \quad A_p = \frac{\omega_{pp}^2}{\omega^2 - \Omega_p^2},$$

so that the dispersion relation in this limit yields

$$A_p^{-1} \approx (1 - A_e)^{-1} - \left(\frac{V_{dp}}{c}\right)^2,$$

or, recalling that $v_A/c \approx \Omega_p/\omega_{pp}$,

$$\left(\frac{\omega}{\Omega_p}\right)^2 \approx 1 - \left(\frac{V_{dp}}{v_A}\right)^2 + \frac{\omega_{pp}^2}{\Omega_p^2}\left(1 + \frac{\omega_{pe}^2}{\Omega_e^2}\right)^{-1}.$$

When, as is the case here, $\omega_{pe}^2 \gg \Omega_e^2$, the last equation simplifies to

$$\left(\frac{\omega}{\Omega_p}\right)^2 \approx \frac{m_p}{m_e} - \left(\frac{V_{dp}}{v_A}\right)^2$$

and explains the behavior encountered in Figure 7. Below the critical value $V_{dp}/v_A \approx (m_p/m_e)^{1/2} = 42.86$, the resonance frequency of the modified extraordinary mode diminishes with increasing drift velocities; beyond this drift threshold, a nonoscillatory instability sets in that, as shown below links with the already discussed parallel propagating purely growing mode.

5. Propagation Off the Principal Directions

[35] The previous results have demonstrated the existence of instabilities when the wave vector is aligned with the principal directions of the adopted frame of reference shown in Figure 1. We now intend to display typical behaviors of those instabilities when the wave vector is allowed to deviate from those orientations, first keeping it in the principal planes and then allowing for a few evolutions free of this constraint.

5.1. Wave Vector in the Drift-Gravity Plane

[36] Here, keeping $\theta = \pi/2$, we follow the evolution of (1) the beam instability found for propagation along the drift direction as the wave vector moves from the y axis to the z axis (Figure 8: $\phi = 0 \rightarrow \pi/2$, $kv_A/\Omega_p = 100$, $V_{dp} = 30v_A$) and (2) the nonoscillatory instability (with the drift threshold determined in the previous section) when the wave vector evolves in the opposite sense, from the z axis to the y axis (Figure 9: $\phi = \pi/2 \rightarrow 0$, $kv_A/\Omega_p = 100$, $V_{dp} = 43v_A$).

[37] The beam instability decreases its real frequency (proportionally to the proton drift velocity component along **k**, that is, $\propto \cos\phi$) and growth rate until quenching sets in (in the depicted case, beyond $\phi = \pi/3$; as implied in Figure 9, quenching is avoided when the drift velocity exceeds the critical value). As soon as the wave vector leaves the z axis in its evolution toward the drift direction, the aperiodic insta-

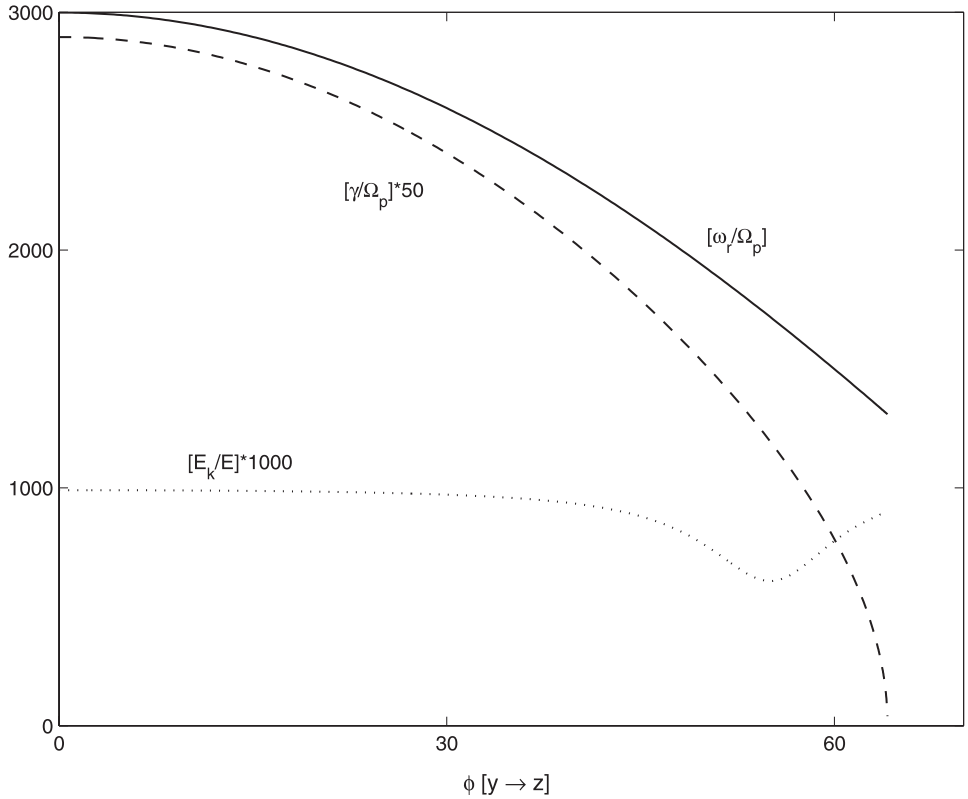

Figure 8. Evolution of the instability encountered in Figure 6 as the wave vector rotates from the y axis to the z axis ($kv_A/\Omega_p = 100$, $V_{dp} = 30v_A$, $\theta = \pi/2$).

bility becomes oscillatory; the real frequency and growth rates increase and smoothly join the beam instability values found for propagation along the y axis.

5.2. Wave Vector in the Drift-Magnetic Field Plane

[38] The adopted procedure is similar to the one used in the previous section. We take $\phi = 0$ and follow the evolution of (1) the beam instability of drift propagation as **k** goes from the y axis to the x axis (Figure 10: $\theta = \pi/2 \rightarrow 0$, $kv_A/\Omega_p = 100$, $V_{dp} = 20v_A$) and (ii) the zero-drift threshold nonoscillatory instability found for parallel ($\theta = 0$) propagation as **k** approaches the drift direction (Figure 11: $\theta = 0 \rightarrow \pi/2$, $kv_A/\Omega_p = 100$, $V_{dp} = 20v_A$).

[39] Again, the real frequency and growth rate of the beam instability decrease as **k** moves away from the y axis with quenching of the instability eventually setting in. As to the aperiodic instability of parallel propagation, it becomes oscillatory as soon as the wave vector departs from the x axis; its growth rate starts to increase with θ and reaches a well-defined maximum just before growth is suppressed. In contrast to the situation described in the drift-gravity field plane where the growing modes found in the corresponding principal axes can reciprocally evolve from one to the other and therefore represent manifestations of the same instability, in this plane the principal axes instabilities are distinct.

5.3. Wave Vector in the Magnetic Field-Gravity Plane

[40] The results obtained in the wave vector evolutions contained in this plane ($\phi = \pi/2$) show that in the realm $\mathbf{k} \cdot \mathbf{V_{ds}} = 0$, that is, for wave vector orientations perpendicular to the drift direction, the existing instabilities nonoscillatory with a growth rate that is almost independent of the **k** direction, provided that the neighbourhood of the gravity direction ($\theta \approx \pi/2$, $\phi \approx \pi/2$) is avoided; here the growth rate very rapidly reaches a minimum that may correspond to stability ($\gamma = 0$) if the drifts are below the threshold deter-

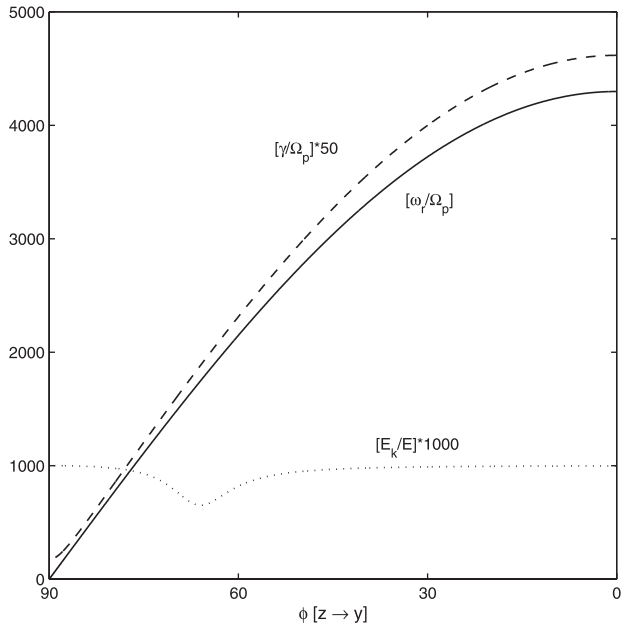

Figure 9. Evolution of the aperiodic instability encountered in Figure 4 as the wave vector rotates from the z axis to the y axis ($kv_A/\Omega_p = 100$, $V_{dp} = 43v_A$, $\theta = \pi/2$).

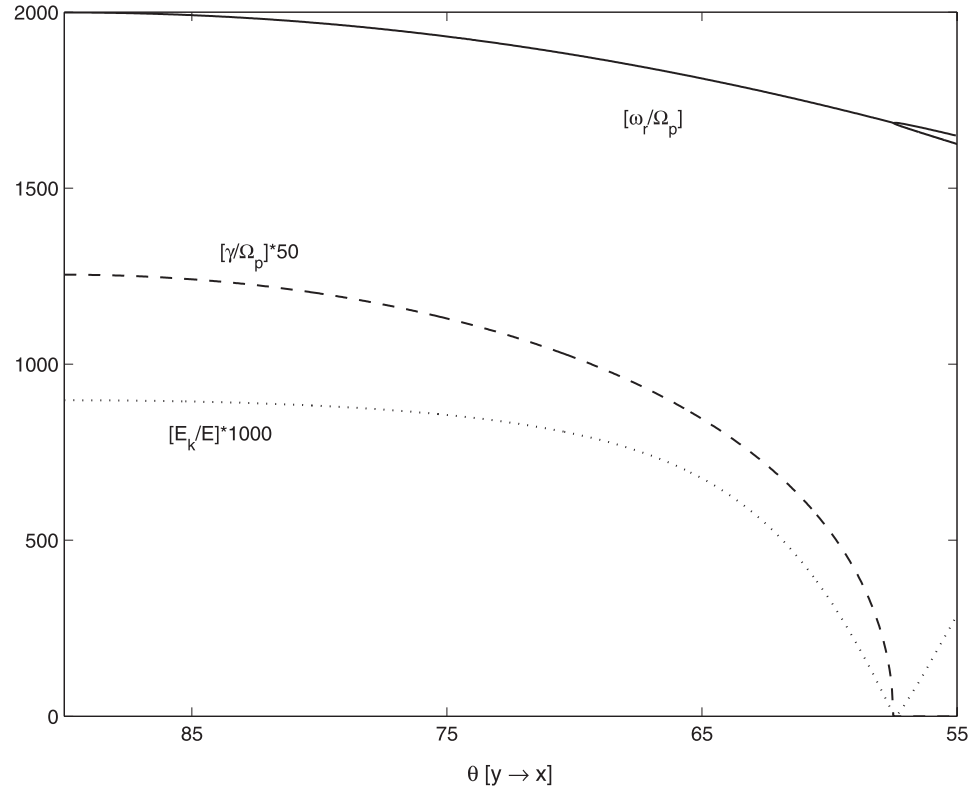

Figure 10. Evolution of the instability encountered in Figure 6 as the wave vector rotates from the y axis to the x axis ($kv_A/\Omega_p = 100$, $V_{dp} = 20v_A$, $\phi = 0$).

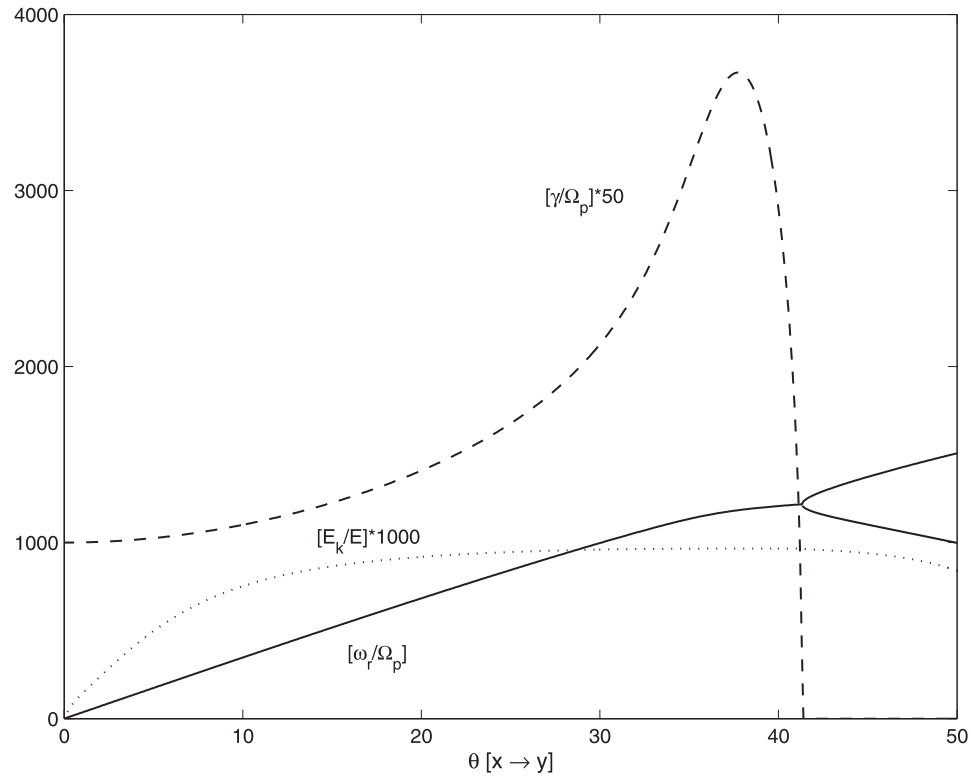

Figure 11. Evolution of the aperiodic instability encountered in Figure 4 as the wave vector rotates from the x axis to the y axis ($kv_A/\Omega_p = 100$, $V_{dp} = 20v_A$, $\phi = 0$).

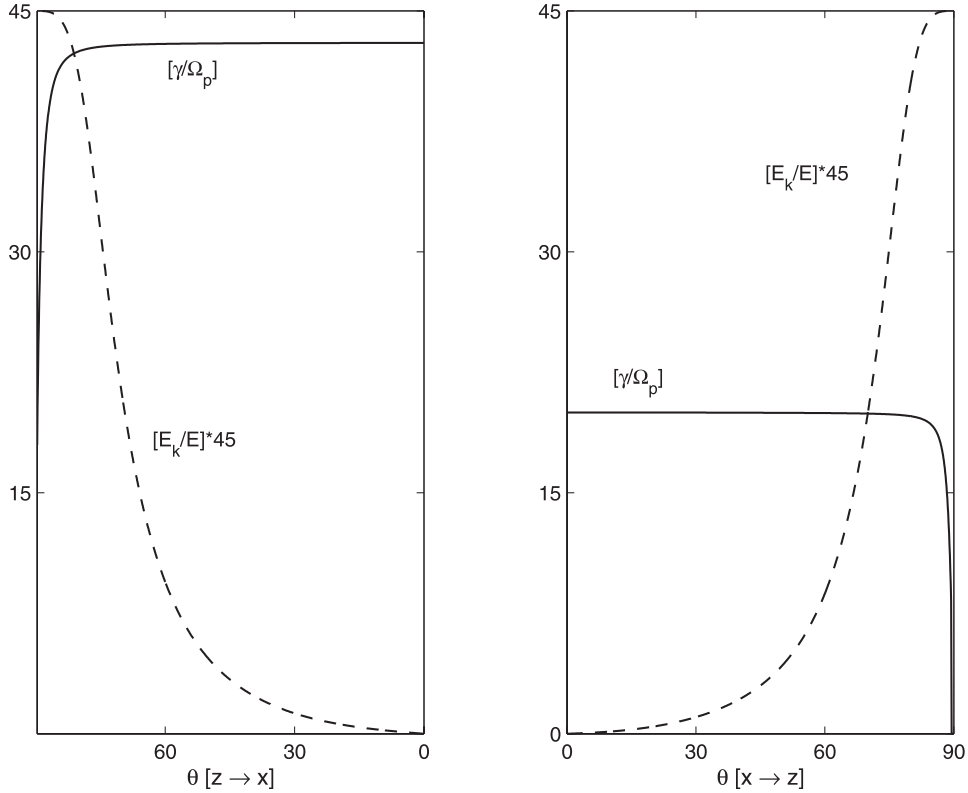

Figure 12. Evolutions of (left) the aperiodic instability encountered in Figure 7 as the wave vector rotates from the z axis to the x axis ($kv_A/\Omega_p = 100$, $V_{dp} = 43v_A$, $\phi = \pi/2$) and (right) the aperiodic instability encountered in Figure 4 as the wave vector rotates from the x axis to the z axis ($kv_A/\Omega_p = 100$, $V_{dp} = 20v_A$, $\phi = \pi/2$).

mined for propagation along the z axis. Figure 12 ($kv_A/\Omega_p = 100$) depicts the growth rates of this aperiodic instability as θ evolves from $\pi/2$ to 0 ($V_{dp} = 43v_A$: just above the z axis threshold) and from 0 to $\pi/2$ ($V_{dp} = 20v_A$: well below the z axis threshold).

5.4. Wave Vector Away From the Principal Planes

[41] Up to now we have only explored the domain ($k_x \geq 0$, $k_y \geq 0, k_z \geq 0$). In a gyrotropic environment the instabilities of the medium would only depend on k and θ. In the envisaged magnetoplasma, however, the introduction of a perpendicular gravity field has broken the gyrotropic symmetry. Here we follow the behavior of two of the previously studied instabilities as the relevant wave vector pursues well-defined evolutions away from the principal planes and, not surprisingly, recover other type of (nongyrotropic) symmetries.

[42] We found in connection with Figure 11 and the nonoscillatory instability for **k** aligned with the ambient magnetic field, as the wave vector (always in the xy-plane) moved away from the x axis in the drift direction, that the growth would become oscillatory, maximize at a certain orientation ($\theta \approx 37.8°$, for the case considered) and be suppressed soon afterward. Figure 13 shows, for this specific value of θ, the dependence of the complex dispersion of the instability on the azimuth angle ϕ (the behavior of gyrotropic media would be independent of this gyrophase-like angle). The growth rate maximizes when the wave vector is aligned with the y direction (notice that, for $k_y < 0$, that is $\cos\phi < 0$, the real frequency ω_r is negative, meaning that the wave phase velocity component along the y direction points in the same direction as the proton drift, thus allowing for the associated wave-particle resonance that feeds the wave growth). Although the instability occurs in the whole azimuthal domain, the growth rate reaches minima when **k** goes through the xz plane and, as already known, turns aperiodic (nonoscillatory).

[43] Figure 14 depicts the characteristics of the same instability when **k** is contained in the azimuthal plane $\phi = \pi/4$ and its colatitude angle θ varies from 0 (positive x axis) to π (negative x axis). The evolution starts with the zero-drift threshold aperiodic instability that immediately becomes oscillatory when the xz plane is left; the growth rate increases initially, maximizes at $\theta \approx 47.6°$ and goes to zero at $\theta \approx 52°$, remaining stable until the symmetric position of this cutoff ($\theta \approx 180 - 52 = 128°$) is attained and the growth history is revisited until the negative x axis is reached and the initial aperiodic instability is recovered (the whole behavior is symmetric with respect to the yz plane).

6. On the Influence of the Neglected Inhomogeneity

[44] We recall that the adopted model neglects the magnetic field generated by the perpendicular current supported by the particle drifts and the associated inhomogeneity of the zero-order medium. Here we assess the effects of this approximation on the discussed instabilities.

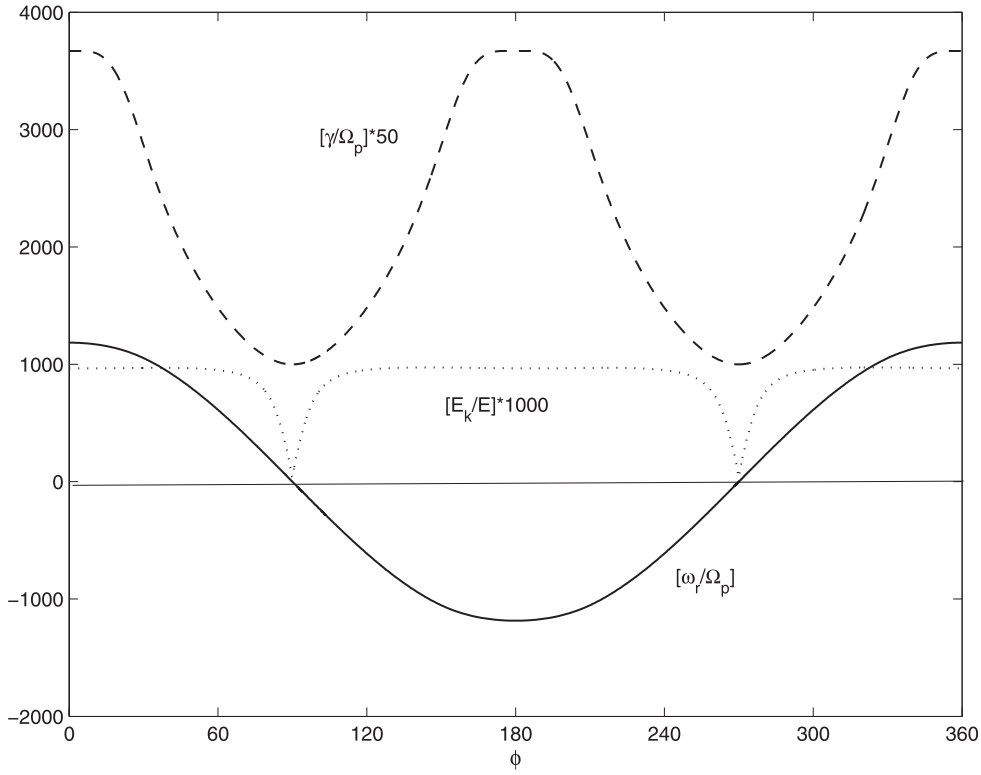

Figure 13. Dependence on the azimuth angle of the instability encountered in Figure 11 at maximum growth rate ($\theta = 37.8°$, $kv_A/\Omega_p = 100$, $V_{dp} = 20v_A$).

[45] These instabilities are basically of two types: (1) the nonoscillatory growth encountered for parallel propagation and its evolution to other directions of propagation, and (2) the ''beam-like'' behavior (essentially electrostatic as the wave number increases) of the wave-particle interactions depicted in Figures 5 and 6 and their extensions to other wave vector orientations. The physical mechanism underlying aperiodic growth was previously discussed in detail, whereas the phenomenology of the beam-plasma interaction is well known, albeit modified here by the zero-order perpendicular magnetic field.

[46] We shall find that the inhomogeneity does not influence 1 and allows for the occurrence of 2.

6.1. Stratified Zero-Order Medium

[47] In the frame of reference of Figure 1 we allow for the possibility of the characteristic parameters of the zero-order equilibrium ($\partial/\partial t = 0$) cold magnetoplasma to depend on the ''vertical'' coordinate z. In the domain of interest the gravity, g, and the population densities, N_{s0}, are uniform, and the particle drifts are aligned with the y axis.

[48] The continuity, momentum, and Maxwell equations are satisfied by the following zero-order equilibrium values of the stratified medium:

$$\mathbf{E}_0 = 0, \quad \sum_s q_s N_{s0} = 0, \quad \mathbf{B}_0 = B_0(z)\mathbf{x},$$

$$\mathbf{V}_{\mathrm{ds0}} = V_{\mathrm{ds0}}(z)\mathbf{y}, \quad V_{\mathrm{ds0}}(z) = \frac{gm_s}{q_s B_0(z)} = \frac{g}{\Omega_s(z)},$$

$$\mathbf{J_0} = J_0(z)\mathbf{y} = \sum_s q_s N_{s0} V_{ds0}(z)\mathbf{y} = \frac{g}{B_0}\sum_s m_s N_{s0}\mathbf{y},$$

with

$$J_0(z) = \sum_s q_s N_{s0} V_{ds0}(z) = \frac{g}{B_0(z)}\sum_s m_s N_{s0} = \frac{gB_0(z)}{\mu_0 v_A^2(z)},$$

$$\frac{\partial B_0}{\partial z} = \mu_0 J_0(z), \quad \text{or} \quad \frac{1}{B_0}\frac{\partial B_0}{\partial z} = \frac{g}{v_A^2} = \frac{1}{L_z},$$

where L_z is the length scale of the vertical inhomogeneity.

6.2. On the New Perturbation Introduced by the Inhomogeneity

[49] With the notation used above and in Appendix A the linearization of the momentum equation yields

$$\frac{\partial \mathbf{v_s}}{\partial t} + V_{ds0}\frac{\mathbf{v_s}}{\partial y} + (\mathbf{v_s}\cdot\nabla)V_{ds0}\mathbf{y} = \frac{q_s}{m_s}(\mathbf{E} + V_{ds0}\mathbf{y}\times\mathbf{B} + \mathbf{v_s}\times\mathbf{B}_0)$$

where the new term introduced by the inhomogeneity (aligned with $\mathbf{y}$) can be estimated by

$$(\mathbf{v_s}\cdot\nabla)V_{ds0} = v_{sz}\frac{\partial V_{ds0}}{\partial z} = v_{sz}g\frac{m_s}{q_s}\frac{\partial}{\partial z}\left(\frac{1}{B_0}\right)$$
$$= -v_{sz}V_{ds0}\frac{\mu_0 J_0}{B_0} = -gv_{sz}\frac{V_{ds0}}{v_A^2},$$

and, apart from other possible terms also aligned with the drift direction, shall combine with $v_{sz}\Omega_s$ that arises from the y component of

$$\frac{q_s}{m_s}\mathbf{v_s}\times\mathbf{B}_0.$$

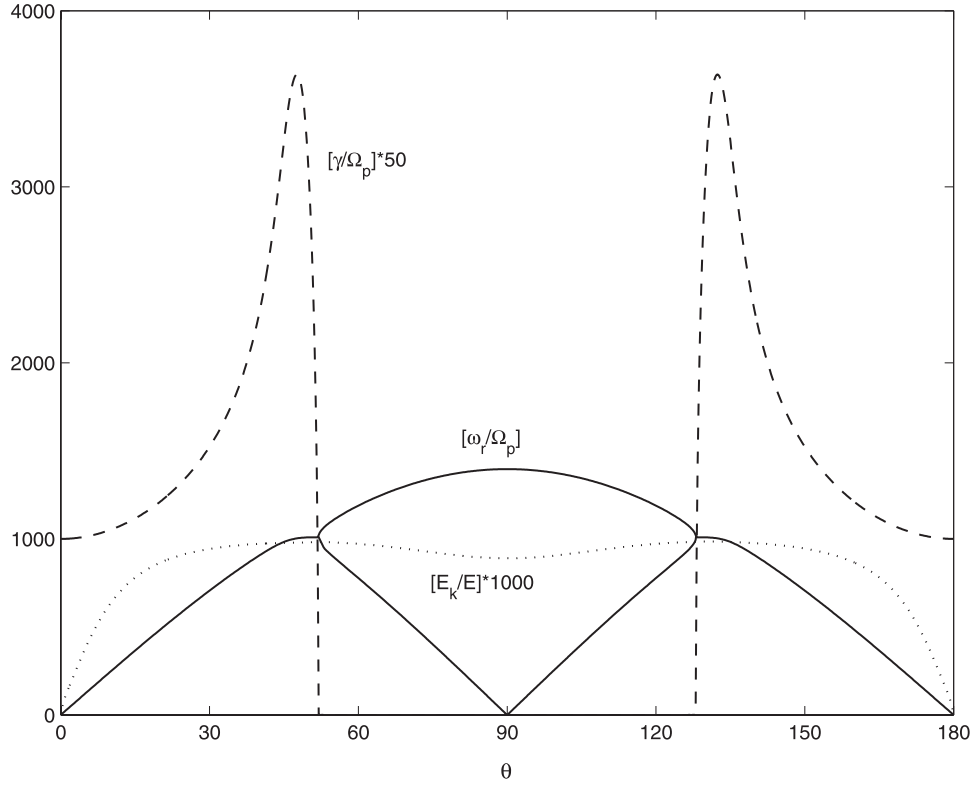

Figure 14. Dependence on the colatitude, at an azimuth $\phi = \pi/4$, of the instability depicted in Figure 13 ($kv_A/\Omega_p = 100$, $V_{dp} = 20v_A$).

6.3. On the Relevance of the New Perturbation

[50] We can thus identify two sufficient (but not necessary) conditions to neglect the influence of the zero-order inhomogeneity in the linear analysis: (1) having $v_{sz} = 0$, or (2) satisfying $V_{ds0}^2 \ll v_A^2$.

[51] Recalling that the detailed analysis of the parallel "propagating" nonoscillatory instability showed that the structure has $v_{sz} = 0$, we conclude that the approximation made in the study of this mode (neglect of the magnetic field generated by the particle drifts and concurrent inhomogeneity) has no influence on the derived results.

[52] As to the beam-like instabilities found for propagation along the drift direction, we can also conclude that the interaction depicted in Figure 5 necessarily satisfies condition 2 above (the resonant heavy ion beam must have a drift speed smaller than the Alfvén speed, so that a fortiori the proton and electron drift speeds will be much smaller than v_A). It remains to be shown that the wave growth depicted in Figure 6 is not a spurious effect of the adopted approximation.

[53] In the spirit of a WKBJ approximation it is possible to proceed with the traditional linear analysis for small-amplitude plane wave perturbations if we restrict the study to wave vectors whose vertical wave numbers satisfy $k_z L_z \gg 1$ and thus assume the first-order quantities $u(\mathbf{r}, t)$ varying as (the real part of) $u(\delta z)\exp[-i(\omega t - \mathbf{k} \cdot \mathbf{r})]$ where $u(\delta z)$ denotes a complex amplitude weakly dependent on z. The issue under analysis, however, does not warrant this full treatment.

[54] Indeed, we note that the modes of Figure 6 propagate along the y direction and become electrostatic as the wave number increases. We can thus focus the attention on large wave numbers and electrostatic perturbations satisfying $J_y - i\omega\varepsilon_0 E_y = 0$ and show that the instability persists. Calculation of the perturbed J_y under these circumstances, with incorporation of the above identified inhomogeneity term, yields the dispersion equation

$$1 = \sum_s \frac{\omega_{ps}^2}{(\omega - kV_{ds0})^2 - \Omega_s^2\left(1 + V_{ds0}^2/v_A^2\right)}$$

that we recognize as a (modified) two-stream interaction dispersion relation where the ratio of the squares of the drift and Alfvén speeds arises from the inhomogeneity, and also has unstable roots.

[55] Just for the sake of illustration, we concentrate on Figure 6, for the case $V_{dp} = 40v_A$ (top right panel). The full analysis for the homogeneous model yields (from the plot) a normalized complex frequency $\omega = 4000. + 84.35$ at the normalized wave number $k = 100.$ whereas the above electrostatic dispersion relation that includes the effects of the inhomogeneity numerically yields, for the same wave number, a similar $\omega = 3998. + 94.63$.

[56] It is thus clear that the instabilities studied in this paper in the framework of the zero-order homogeneous medium with the neglect of the magnetic field caused by the perpendicular particle drifts are not artifacts of the adopted approximation: consideration of a zero-order stratified medium generated by this (previously ignored) magnetic field does not quench the wave growths encountered in the uniform model.

7. Discussion

[57] The investigation of the stability of the assumed cold magnetoplasma has shown that the free energy available in the perpendicular particle drifts can feed a variety of growing wave modes with frequencies well below the upper hybrid resonance. The adopted approach created the particle drifts permeating the magnetoplasma with a perpendicular gravity field but the results are applicable to perpendicular drifts generated by other mechanisms; it permits consideration of arbitrary orientations of the wave vector, cold plasma populations, and drift speeds (within the limits of validity of a non relativistic treatment). The study of the dependence of the instabilities on the drift magnitude and the wave vector orientation has shown that some of them are strongly resilient, with zero-drift thresholds both for aperiodic and oscillatory growing modes.

[58] To assess the effects of the only inconsistency of the adopted cold plasma model (neglect of the magnetic field generated by the zero-order perpendicular current and the associated nonuniformity of the medium) we have treated in an approximate manner a (zero-order) self-consistent stratified cold magnetoplasma. We found that the inhomogeneity has no influence on the encountered nonoscillatory instability for propagation along the background magnetic field (this growth extends to other wave vector orientations in the *xz* plane), and does not quench the other instabilities (along the drift direction and corresponding extensions) that are manifestations of well-known wave-particle interactions (e.g., Figure 5) and/or beam-like behavior (e.g., Figure 6) originated in the drifting populations. Therefore the instabilities encountered for the homogeneous medium in the main part of this investigation are not artifacts of the approximation introduced in the zero-order model.

[59] Similar configurations have been studied for restricted orientations of the wave vector and layered (usually, albeit not always, discontinuous at the boundaries) media. Some of the conclusions might seem identical, but, in general, closer scrutiny is warranted. For example, the Kruskal-Schwarzschild [*Kruskal and Schwartzschild*, 1954] aperiodic flute instability in a magnetoplasma permeated by a gravity field (a close relative of the classical Rayleigh-Taylor instability of a heavy fluid supported by a light fluid) might look as the nonoscillatory growth found in several instances of our study. Interestingly, its occurrence relies on the orientation of $\mathbf{k}$ along the drift direction (or at least having $k_y \neq 0$), the very same condition that in our environment quenches the aperiodic growth. Solution of the apparent contradiction arises from the recognition that the above flute instability takes place in a surface wave located at the boundary (perpendicular to the gravity field) separating two distinct media, whereas our model is thoroughly homogeneous and thus supports no such boundary and therefore wave. In this respect, we reiterate that we did not address here the problem of the stability of a magnetoplasma-gravity system. The gravity field was only a simple means of generating perpendicular particle drifts (that could have been created by other mechanisms) whose stability was then studied.

[60] In the context of space plasmas, the investigated configuration could provide a zero-order model of equatorial planetary magnetospheres. As already stressed, however, this first stage of the study of the stability of perpendicular currents is not concerned with specific applications. Rather, the obtained results provide a reference structure that shall guide the next step of the investigation, when a kinetic approach is envisioned and the ensuing complexity (namely, ion and electron Bernstein modes, thermal cyclotron and Landau damping, higher order cyclotron resonances, transcendental dispersion equations) recommends proper orientation. We shall then have available a model that can be adapted to the study of other situations and environments.

[61] Indeed, we do not anticipate relevant results arising from direct applications of the model to planetary magnetospheres. In the case of the Earth, for $L \approx 4$, we obtain proton gravity drift speeds around 1 cm s^{-1} and Alfvén speeds (even within the plasmasphere) several orders of magnitude larger. Going to Jupiter, the surface gravity is only $\sim$2.5 times larger that at Earth's surface but the associated Jovian magnetic field is more than an order of magnitude larger; of course, the situation improves at larger altitudes because the gravity force only decays with L_J^{-2}, whereas the (assumed dipolar) Jovian field (and the Alfvén speed, for invariant density) falls with L_J^{-3}, but, even at $L_J \approx 50$, the proton gravity drift is only of the order of 3 cm s^{-1}.

[62] The potential spatial applications of this study, after its extension to more realistic hot plasmas, lie in environments whose perpendicular currents arise from mechanisms other than the gravitational drift. For example, without neglecting the effects of the ambient magnetic field on the beam particles, the approach can study the effects of ion injection in space, as in the experiment described by *Kintner and Kelley* [1983], or use the well-known analogy between gravity drifts and other differently originated drifts [e.g., *Mikhailovskii*, 1974] to investigate the effects of curvature of the magnetic lines of force, density and field gradients, and high-frequency forces. Elsewhere in the solar system, as already mentioned in the introduction, another mechanism contributing to particle drifts in the giant planets arises from the centrifugal force; at Jupiter, the ratio between the centrifugal and gravitational forces is given by $(2\pi/T_J)^2(r_J/g_J)L_J^3 \approx 0.1\ L_J^3$, where T_J denotes the Jovian rotational period (0.41 Earth days): it is clear that at large L_J the centrifugal drift becomes (very strongly) dominant.

Appendix A: The Wave Matrix Equation

[63] The cold magnetoplasma under consideration is made up of an arbitrary number of particle populations identified with the subscript s and permeated by a gravity field with the geometry depicted in Figure 1. The zero-order state has species with number densities N_s drifting with velocities $\mathbf{V_{ds}}$ defined below and is charge neutral. The magnetic field generated by the particle drifts is neglected. The linearized Maxwell, Lorentz, and continuity equations describe the behavior of the plane wave perturbations ($\mathbf{E}$, $\mathbf{B}$, $\mathbf{J}$, n_s, $\mathbf{v_s}$) varying as $\exp[-i(\omega t - \mathbf{k}\cdot\mathbf{r})]$,

$$\mathbf{k}\times\mathbf{B} = -i\mu_0\mathbf{J} - \frac{\omega}{c^2}\mathbf{E},$$

$$\mathbf{k}\times\mathbf{E} = \omega\mathbf{B},$$

$$-i(\omega - \mathbf{k}\cdot\mathbf{V_{ds}})\mathbf{v_s} = \frac{q_s}{m_s}\mathbf{E} + \frac{q_s}{m_s}\mathbf{V_{ds}}\times\mathbf{B} + \Omega_s\mathbf{v_s}\times\mathbf{x},$$

$$\mathbf{k}\cdot\mathbf{J_s} = \omega q_s n_s,$$

where

$$\mathbf{J} = \underline{\sigma} \cdot \mathbf{E} = \sum_s \mathbf{J_s} = \sum_s q_s (N_s \mathbf{v_s} + n_s \mathbf{V_{ds}}),$$

$\mathbf{V_{ds}} = (g/\Omega_s)\mathbf{y}$ denote the drift velocities, $\Omega_s = q_s B_0/m_s$ represents the signed angular cyclotron frequency of species s, $\underline{\sigma}$ stands for the conductivity tensor, and other notation is standard.

[64] These relations allow for the derivation of the wave matrix equation

$$\left(\frac{k^2c^2}{\omega^2} - 1\right)\mathbf{E} - \frac{c^2}{\omega^2}(\mathbf{k}\cdot\mathbf{E})\mathbf{k} - i\frac{1}{\omega\varepsilon_0}\underline{\sigma}\cdot\mathbf{E} \equiv \underline{\mathbf{M}}\cdot\mathbf{E} = 0.$$

Using $\mathbf{k} = \mathbf{k}_\perp + k_x\mathbf{x}$ where (Figure 1) $k_\perp = k\sin\theta$, $k_x = k\cos\theta$, $k_y = k_\perp \cos\phi$, $k_z = k_\perp \sin\phi$, the wave matrix elements M_{ij} become

$$M_{xx} = \frac{(k^2 - k_x^2)c^2}{\omega^2} - 1 + \sum_s \frac{\omega_{ps}^2}{\omega^2}$$

$$M_{xy} = M_{yx} = -\frac{k_x k_y c^2}{\omega^2} + \sum_s \frac{k_x V_{ds}}{\omega_s}\frac{\omega_{ps}^2}{\omega^2}$$

$$M_{xz} = M_{zx} = -\frac{k_x k_z c^2}{\omega^2}$$

$$M_{yy} = \frac{\left(k^2 - k_y^2\right)c^2}{\omega^2} - 1 + \sum_s \left[\frac{\omega_{ps}^2}{\omega_s^2 - \Omega_s^2}\left(1 + \frac{k_z^2 V_{ds}^2}{\omega^2}\right) + \frac{k_x^2 V_{ds}^2 \omega_{ps}^2}{\omega^2\omega_s^2}\right]$$

$$M_{yz} = -\frac{k_y k_z c^2}{\omega^2} + \sum_s \frac{\omega_{ps}^2}{\omega_s^2 - \Omega_s^2}\left(i\frac{\Omega_s}{\omega} + \frac{\omega_s k_z V_{ds}}{\omega^2}\right)$$

$$M_{zy} = -\frac{k_y k_z c^2}{\omega^2} + \sum_s \frac{\omega_{ps}^2}{\omega_s^2 - \Omega_s^2}\left(-i\frac{\Omega_s}{\omega} + \frac{\omega_s k_z V_{ds}}{\omega^2}\right)$$

$$M_{zz} = \frac{(k^2 - k_z^2)c^2}{\omega^2} - 1 + \sum_s \frac{\omega_s^2 \omega_{ps}^2}{\omega^2\left(\omega_s^2 - \Omega_s^2\right)}$$

with $\omega_s = \omega - k_y V_{ds}$.

[65] These matrix elements can be used to obtain the wave electric field ratios E_i/E_j and thus calculate the quotient

$$\frac{E_k}{E} = \frac{|\mathbf{k}\cdot\mathbf{E}|}{kE} \tag{70}$$

that assesses the relative electrostatic component of the total wave electric field and is plotted in some figures.

[66] **Acknowledgments.** This work was partially supported by ICCTI/CONICYT. Michel Blanc thanks Gerard Belmont, Karl-Heinz Glassmeier, and another referee for their assistance in evaluating this paper.

References

Brinca, A. L., and F. J. Romeiras, On the stability of stationary nongyrotropic distribution functions: Coupling and purely growing waves, *J. Geophys. Res.*, *103*, 9275–9283, 1998.

Brinca, A. L., L. Borda de Agua, and D. Winske, Nongyrotropy as a source of instability and mode coupling, *Geophys. Res. Lett.*, *19*, 2445–2448, 1992.

Brinca, A. L., L. Borda de Agua, and D. Winske, On the stability of nongyrotropic ion populations: A first (analytic and simulation) assessment, *J. Geophys. Res.*, *98*, 7549–7560, 1993.

Ferrière, K. M., C. Zimmer, and M. Blanc, Magnetohydrodynamic waves and gravitational/centrifugal instability in rotating systems, *J. Geophys. Res.*, *104*, 17,335–17,356, 1999.

Harris, E. G., On a plasma sheath separating regions of oppositely directed magnetic field, *Nuovo Cimento A-B*, *23*, 115–121, 1962.

Kintner, P. M., and M. C. Kelley, A perpendicular ion beam instability: Solutions to the linear dispersion relation, *J. Geophys. Res.*, *88*, 357–364, 1983.

Kruskal, M., and M. Schwartzschild, Some instabilities of a completely ionized plasma, *Proc. R. Soc. London, Ser. A*, *223*, 348–360, 1954.

Lee, L. C., and J. R. Kan, A unified kinetic model of the tangencial magnetopause structure, *J. Geophys. Res.*, *84*, 6417–6426, 1979.

Lehnert, B., Gravitational instability of a magnetized plasma, *Phys. Rev. Lett.*, *7*, 440–441, 1961.

Lominadze, D. G., Cyclotron instabilities in plasma with a transverse current, in *Cyclotron Waves in Plasma*, chap. 2, Pergamon, New York, 1981.

Mikhailovskii, A. B., Plasmas in a gravitational field, in *Theory of Plasma Instabilities*, vol. 2, chap. 6, Consult. Bur., New York, 1974.

Motschmann, U., and K.-H. Glassmeier, Relation of magnetic field line reconnection and unstable nongyrotropic particle distributions, in *International Conference on Substorms-4*, edited by S. Kokubun and Y. Kamide, p. 491, Kluwer Acad., Norwell, Mass., 1998.

Wu, C. S., Y. M. Zhou, S. T. Tsai, S. C. Guo, D. Winske, and K. Papadopoulos, A kinetic cross-field streaming instability, *Phys. Fluids*, *26*, 1259–1267, 1983.

A. L. Brinca and F. J. Romeiras, Centro de Física de Plasmas, Instituto Superior Técnico, Lisbon 1049-001 Portugal. (ebrinca@alfa.ist.utl.pt; filipe.romeiras@math.ist.utl.pt)

L. Gomberoff, Departamento de Física, Facultad de Ciencias, Universidad de Chile, Casilla 653, Las Palmeras 3425, Santiago, Chile. (lgombero@uchile.cl)